LETTER

https://doi.org/10.1038/s41586-019-1308-y

Helical van der Waals crystals with discretized Eshelby twist

Yin Liu[1,2,9], Jie Wang[3,9], Sujung Kim[1,8,9], Haoye Sun[1,9], Fuyi Yang[1,2], Zixuan Fang[1,4], Nobumichi Tamura[5], Ruopeng Zhang[1,6], Xiaohui Song[6], Jianguo Wen[3], Bo Z. Xu[1], Michael Wang[1], Shuren Lin[1,2], Qin Yu[2], Kyle B. Tom[1,2], Yang Deng[1], John Turner[6], Emory Chan[7], Dafei Jin[3], Robert O. Ritchie[1,2], Andrew M. Minor[1,6], Daryl C. Chrzan[1,2], Mary C. Scott[1,6] & Jie Yao[1,2]*

The ability to manipulate the twisting topology of van der Waals structures offers a new degree of freedom through which to tailor their electrical and optical properties. The twist angle strongly affects the electronic states, excitons and phonons of the twisted structures through interlayer coupling, giving rise to exotic optical, electric and spintronic behaviours[1–5]. In twisted bilayer graphene, at certain twist angles, long-range periodicity associated with moiré patterns introduces flat electronic bands and highly localized electronic states, resulting in Mott insulating behaviour and superconductivity[3,4]. Theoretical studies suggest that these twist-induced phenomena are common to layered materials such as transition-metal dichalcogenides and black phosphorus[6,7]. Twisted van der Waals structures are usually created using a transfer-stacking method, but this method cannot be used for materials with relatively strong interlayer binding. Facile bottom-up growth methods could provide an alternative means to create twisted van der Waals structures. Here we demonstrate that the Eshelby twist, which is associated with a screw dislocation (a chiral topological defect), can drive the formation of such structures on scales ranging from the nanoscale to the mesoscale. In the synthesis, axial screw dislocations are first introduced into nanowires growing along the stacking direction, yielding van der Waals nanostructures with continuous twisting in which the total twist rates are defined by the radii of the nanowires. Further radial growth of those twisted nanowires that are attached to the substrate leads to an increase in elastic energy, as the total twist rate is fixed by the substrate. The stored elastic energy can be reduced by accommodating the fixed twist rate in a series of discrete jumps. This yields mesoscale twisting structures consisting of a helical assembly of nanoplates demarcated by atomically sharp interfaces with a range of twist angles. We further show that the twisting topology can be tailored by controlling the radial size of the structure.

Many crystals can be grown into twisted forms on scales ranging from nanoscale to mesoscale and macroscale[8–14]. Specifically, an axial screw dislocation in a one-dimensional structure can produce a continuous crystallographic twist, known as the Eshelby twist, giving rise to helically twisted nanowire structures[15,16]. This mechanism potentially provides a means to create twisted van der Waals (vdW) structures. Materials such as germanium sulfide (GeS) can grow into nanowires along the vdW stacking direction (the cross-plane direction)[17–20], and introducing Eshelby twist into such nanowires naturally leads to twist between the successive layers. Even though screw dislocations in layered vdW materials are well known[21–23], the Eshelby twist has not been considered in those materials. Here we report the observation of the Eshelby twist in vdW materials and show how this enables the synthesis of vdW structures with various twisting morphologies. This approach opens new possibilities for creating twisted vdW structures with tailored topologies.

The synthesis method was demonstrated using GeS, a layered IV–VI monochalcogenide. Twisted GeS structures were synthesized on silicon substrates with a 3–4 nm native oxidized layer by using a chemical vapour transport method with gold as a catalyst (see Methods and Extended Data Fig. 1). A representative scanning electron microscopy (SEM) image of a mesoscale crystal is presented in Fig. 1a, showing a well-defined helicoidal morphology. The synthesized crystals have varying twist periods ranging from 2 μm to 20 μm, with total lengths up to hundreds of micrometres, and radial sizes ranging from several hundred nanometres to more than 10 μm. They have a three-dimensional architecture consisting of periodically rotating nanoplates with a thickness of several hundred nanometres, as is revealed by cross-sectional transmission electron microscopy (TEM) (Fig. 1b) and cross-sectional SEM images acquired through consecutive focused ion beam milling along the twist axis (Fig. 1d, Supplementary Video 1). Statistical analysis suggests approximately equal numbers of left-handed and right-handed crystals (Extended Data Fig. 2). Quantitative chemical analysis of the structure indicates a 1:1 atomic ratio of Ge:S (Extended Data Fig. 2). The crystallography is revealed through synchrotron X-ray Laue microdiffraction analysis with submicrometre spatial resolution[24]. X-ray crystal orientation maps of the structures (Fig. 1e, f, Extended Data Fig. 2) show that the twist axis of the crystal is along the *c* axis (the cross-plane direction), and the vdW planes, defined by the *a* and *b* axes in Fig. 1c, periodically rotate about the *c* axis such that there is a total twist of 180° in a single period (that is, between two adjacent minimum widths as seen in Fig. 1a).

Atomic-resolution scanning transmission electron microscopy (STEM) suggests that the nanoplates are single crystals in the space group *Pcmn* and that the twist interface between the nanoplates is atomically sharp (Fig. 2a, Extended Data Fig. 2). The twist angle at this interface is 10.27° (as determined from the change of tilt angle needed to tilt each of the two crystals to the [010] zone axis; Fig. 2a, b). The twist interface was also characterized by plan-view TEM of the stacking nanoplates with the incident electron beam along the twist axis (Fig. 2c–e, Extended Data Fig. 3). Electron diffraction patterns indicate a misorientation angle of 7.5° between the two nanoplates (Fig. 2c, d), and double diffraction patterns were clearly observed from the twist boundary (Fig. 2e). The double diffraction in reciprocal space reflects long-range ordering with a period of 2.26 nm in real space, which agrees well with the simulated rotational moiré pattern (Fig. 2f, g). In addition to TEM, we used electron backscattering diffraction to measure twist angles (Extended Data Fig. 4). In total, 15 twist angles in several structures were quantified, ranging from 6.8° to 16° with an average of 10.3°. Further estimates of the twist angles were based on

[1]Department of Materials Science and Engineering, University of California Berkeley, Berkeley, CA, USA. [2]Materials Sciences Division, Lawrence Berkeley National Laboratory, Berkeley, CA, USA. [3]Center for Nanoscale Materials, Nanoscience and Technology Division, Argonne National Laboratory, Lemont, IL, USA. [4]National Engineering Research Center of Electromagnetic Radiation Control Materials, University of Electronic Science and Technology of China, Chengdu, China. [5]Advanced Light Source, Lawrence Berkeley National Laboratory, Berkeley, CA, USA. [6]National Center for Electron Microscopy, Molecular Foundry, Lawrence Berkeley National Laboratory, Berkeley, CA, USA. [7]Molecular Foundry, Lawrence Berkeley National Laboratory, Berkeley, CA, USA. [8]Present address: Department of Electrical and Computer Engineering, University of California Santa Cruz, Santa Cruz, CA, USA. [9]These authors contributed equally: Yin Liu, Jie Wang, Sujung Kim, Haoye Sun. *e-mail: yaojie@berkeley.edu

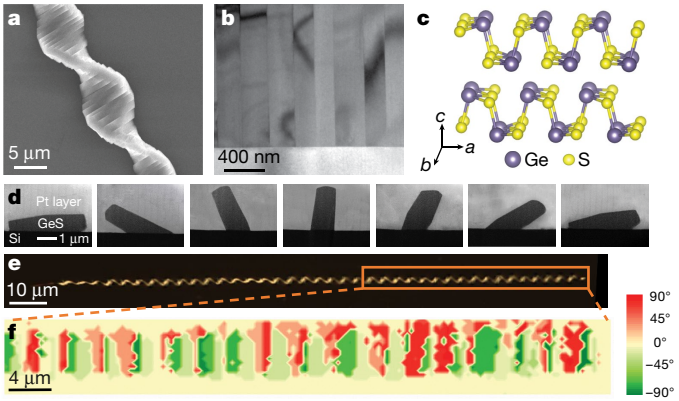

Fig. 1 | Structure of mesoscale twisted GeS crystals. a, SEM image showing the twisting morphology of a mesoscale GeS crystal. **b**, Cross-sectional TEM image of a twisted crystal. The surface normal of the cross-section is perpendicular to the twist axis. **c**, Layered crystal structure of GeS. **d**, A series of SEM images showing the evolution of radial cross-sections within one period of a twisted structure. **e**, **f**, Optical micrograph (**e**) and crystal orientation map (**f**) of a twisted structure generated by X-ray Laue microdiffraction analysis. The orientation angle is defined by the angle between the *b* axis and the norm of the substrate. The region of the X-ray analysis is highlighted by the orange box in **e**.

the number of nanoplates or interfaces per period, obtained from SEM imaging. The distribution of twist angles obtained this way (Fig. 2h) is in good agreement with the direct measurements.

Next, we show that this mesoscopic twist originates from Eshelby twist in the dislocated nanowires that were first grown via the gold-catalysed vapour–liquid–solid (VLS) method (Fig. 3a, b). In contrast to the VLS growth of GeS nanowires in previous studies[17,18], we observed GeS nanowires with continuous morphological twists (Fig. 3c), reminiscent of the Eshelby twist in non-vdW materials[10,11]. Eshelby predicted that an axial screw dislocation at the centre of a thin whisker will result in a twist that relieves the elastic energy associated with the screw dislocation[16]. The twist rate is $\alpha = \kappa b/A$ where b is the magnitude of the Burgers vector $\boldsymbol{b}$ of the screw dislocation, κ is a prefactor related to the geometry of the whisker, and A is the cross-sectional area of the whisker. To grow nanowires with the Eshelby twist, we had to optimize growth parameters including pressures and carrier gas flow rates (see Methods); for non-optimal growth conditions, almost all of the synthesized nanowires are synthesized with no twist (Extended Data Fig. 5).

We confirmed the existence of the Eshelby twist through TEM studies. In TEM (Fig. 3d) and high-resolution TEM images (Fig. 3e), a line defect is evident at the centre of the nanowire. Convergent beam electron diffraction (CBED) shows that the nanowire has a crystallographic twist (Fig. 3d), giving rise to 24° of rotation about the *c* axis over an approximate distance of 1.4 μm. This amounts to a twist rate of 0.3 rad μm^{-1}, comparable to the twist rates reported in nanowires of conventional covalent semiconductors[10,11]. Burgers vector analysis was performed on the basis of $\boldsymbol{g} \cdot \boldsymbol{b}$ contrast in TEM images (Fig. 3f–i): the dislocation is imaged with different $\boldsymbol{g}$ reflections in reciprocal space and becomes invisible when $\boldsymbol{g} \cdot \boldsymbol{b} = 0$. Dark-field images were taken for $\boldsymbol{g} = (002)$ and $\boldsymbol{g} = (\bar{2}10)$ for a strong two-beam condition near the [210] zone axis. At $\boldsymbol{g} = (002)$, high contrast of the dislocation was observed, whereas for $\boldsymbol{g} = (\bar{2}10)$, the dislocation became invisible. As such, the direction of Burgers vector is determined to be along the [001] growth direction (*c* axis), confirming the screw character of the dislocation.

Further radial growth on those nanowires with the Eshelby twist results in mesoscale twisted GeS (Fig. 4a). We found that the gold nanoparticle that catalyses the VLS growth of the nanowire was present at the tip of the mesoscale structure (Fig. 4b), with a size proportional to the period of the structure; here, a large catalyst particle corresponds to a large period. The twist rates of the mesoscale structures are 0.2–1.1 rad μm^{-1}, comparable to the measured twist rate of the GeS nanowire. Further analysis established a good linear relationship between the overall twist rate of the mesoscale structure and the inverse

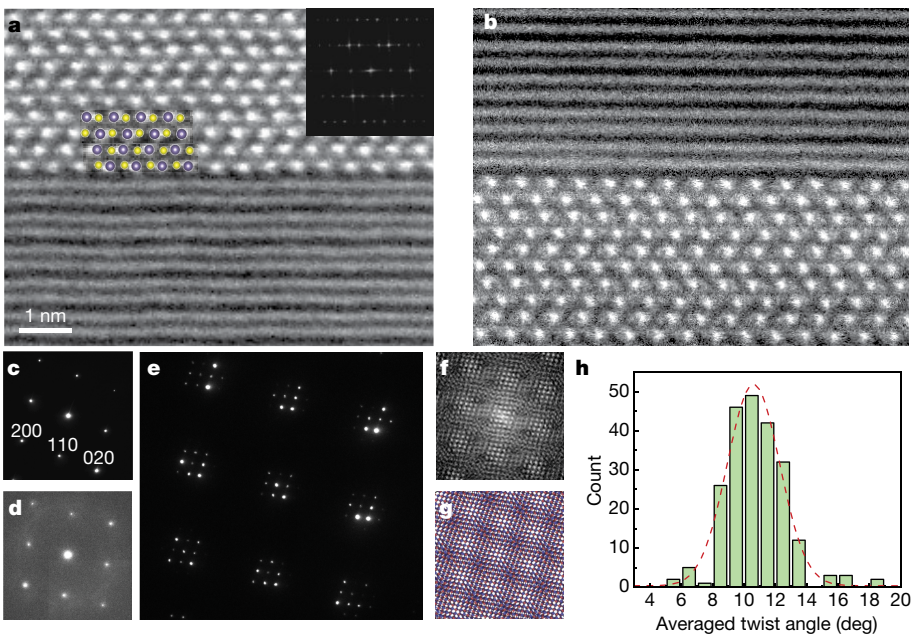

Fig. 2 | Twist interfaces and twist angles in mesoscale GeS structures. **a**, High-angle annular dark-field scanning transmission electron microscopy (HAADF-STEM) image showing the atomically sharp interface between two nanoplates in a twisted structure with the upper crystal on the [010] zone axis. A structural model of GeS with labelled Ge atoms (blue) and S atoms (yellow) is superimposed on the STEM image. The inset shows the fast Fourier transform (FFT) pattern of the upper crystal. **b**, HAADF-STEM image of the same interface with the lower crystal on the [010] zone axis. **c**, **d**, Selected area electron diffraction (SAED) patterns for the [001] zone axis acquired from a plan-view TEM sample (see also Extended Data Fig. 3) containing two stacking nanoplates. SAED patterns were acquired on the top crystal (**c**) and bottom crystal (**d**), suggesting a misorientation angle of 7.5° between those two crystals. **e**, Double diffraction pattern acquired from the twist interface of the two nanoplates. **f**, **g**, Inverse FFT images of the double diffraction pattern (**f**) and the simulated rotational moiré pattern (**g**), illustrating the long-range periodicity in real space. **h**, Distribution of twist angle estimated by counting the number of interfaces per period using SEM imaging.

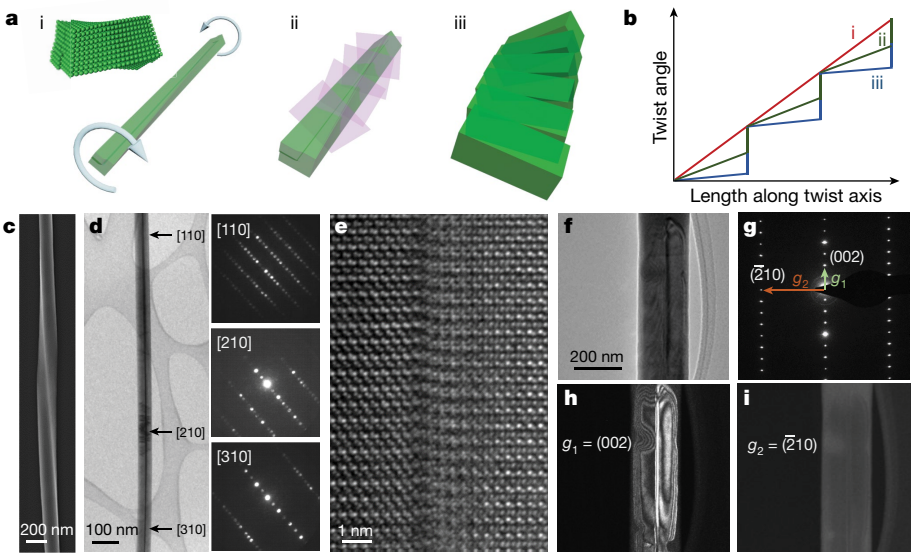

Fig. 3 | GeS nanowires with Eshelby twist. a, Schematics showing the formation mechanism of the mesoscale GeS structures with discrete twisting. i, The growth of nanowire with Eshelby twist. The inset shows a schematic of the atomic structure of the Eshelby twist. ii, Interlayer slip that forms the twist grain boundary. iii, Further radial growth giving rise to the discretely twisting morphology. **b**, Schematic diagram showing the twisting profile transitions from a continuous twist to a discrete twist, corresponding to states i–iii in **a**. **c**, SEM image of a twisted nanowire adhering to a substrate. **d**, TEM image of a nanowire with Eshelby twist (left) and corresponding CBED patterns (right) taken from different locations on the nanowires, suggesting that the crystal orientation changes from direction [110] to [210] and then to [310] with respect to the incident electron beam. The locations are marked with black arrows. Note the CBED patterns are rotated 38° anticlockwise with respect to the image of the nanowire. **e**, High-resolution TEM image of the dislocation. **f**, TEM image of another nanowire with axial dislocation tilted on the [120] zone axis. **g**, Corresponding SAED pattern for the nanowire in **f** . The arrows in the SAED pattern highlight the reflections used for $\boldsymbol{g}\cdot\boldsymbol{b}$ analysis. **h**, **i**, Dark-field TEM images under the two-beam condition showing high (**h**) and low (**i**) contrast of the dislocation when $\boldsymbol{g}_1 = (002)$ and $\boldsymbol{g}_2 = (\bar{2}10)$ are excited, respectively.

of the cross-sectional area of the catalyst particle at its contact with GeS. The size of the catalyst particle at the tip of mesoscale structures approximately represents the radial size of the nanowires first axially grown by the VLS process (Fig. 4c). The relationship between the twist rate and catalyst size effectively reflects the relationship between the twist rate and cross-sectional area of the VLS-grown nanowires (Fig. 4f), revealing the Eshelby twist mechanism underpinning the formation of the discretely twisting structure. Fitting of the results using the Eshelby model gives a reasonable magnitude of 1.75 nm for κb, which is between one and two lattice constants along the c axis ($c = 1.04$ nm). This magnitude agrees with the fact that the Burgers vector tends to be the shortest lattice vector (c) to reduce the elastic energy. For a more accurate evaluation of the Burgers vector from the Eshelby model, the anisotropic crystal structure and the complex cross-section of the nanowire should be considered, to correct the overestimation of area arising from our assumption of a circular cross-section and to determine the prefactor κ (ref. [15]).

Although the Eshelby twist is essential, it cannot completely account for the discretization of the mesoscopic twist. For free-standing nanowires, radial growth increases the rigidity of the material, which counteracts the torque applied by the axial dislocation, resulting in the untwisting of the nanowire. This untwisting is in agreement with Eshelby's theory, which shows that the twist rate inversely scales with the cross-sectional area, so that at a radius of a few micrometres, in the Eshelby model, the twist rate becomes negligible[15]. Thus, the high twist rates in the mesoscale twisted GeS that are comparable to the twist rate of dislocated nanowires cannot be interpreted through the Eshelby model alone. The key to the formation of the discretized twisting in the structure is the interaction of the dislocated nanowire with the substrate. During growth, some of the free-standing dislocated nanowires adhere to the substrate. Unlike the free-standing nanowires, further radial growth of the nanowires pinned by the substrate does not result in untwisting, and the high twist rate of the initial nanowire would thus be preserved. This invariance in the twist rate with radial growth is the mechanism that permits us to detect the Eshelby twist in mesoscale GeS (Fig. 4f). Our experiments (Extended Data Fig. 6) verify that the overall twist rate of a pinned structure remains almost constant with increasing radial size, and the twist rate of the mesoscale structure equals the twist rate of the initial nanowire upon substrate pinning.

Without the freedom to untwist, the volumetric elastic strain energy of the pinned nanowires rapidly builds up with radial growth. At a critical radial size, rotational slip of atomic layers is enabled by the weak interlayer vdW bonding in GeS to relieve the strain energy, resulting in the formation of twist boundaries and the discretization of the structure. The reduction of strain energy is counteracted by the increase in interfacial energy associated with the twisted interfaces, and this interplay defines the final twisting morphology. The elastic strain energy of the mesoscale structure is revealed by photoluminescence measurements (Fig. 4d, e). The photoluminescence emission peak is redshifted by 30 meV (from 748 nm to 766 nm) from the outer region, where the photoluminescence emission is consistent with the emission of strain-free GeS (1.65eV)[25], to the central region of the structure. This result indicates the existence of torsional strain around the centre of the structure, in accordance with modification of bandgaps induced by screw dislocations as suggested in previous studies[26,27].

To illustrate this energy competition, we theoretically calculated the change in total energy, ΔE_{tot}, for each segment of the nanowire of length Δl, upon introducing a twist boundary into a pinned nanowire with a twist rate defined by the initial radius R_{i} of the nanowire upon its adhesion to the substrate (see Methods). We propose that ΔE_{tot} has two contributions, $\Delta E_{\mathrm{tot}} = \Delta E_{\mathrm{elastic}} + \Delta E_{\mathrm{dis}}$, namely, a term $\Delta E_{\mathrm{elastic}}$ due to the change in elastic energy in each segment of the wire with length Δl, and a term ΔE_{dis} due to the introduction of the misfit dislocations defining a twist boundary. The $\Delta E_{\mathrm{elastic}}$ is found to be dependent on both the spacing between the twist boundaries Δl and the radial size of the pinned nanowire. Figure 4g displays ΔE_{tot} for a pinned nanowire with $R_{\mathrm{i}} = 36$ nm as a function of Δl for three different values of radius. The result suggests a critical radius R_{c}, above which it becomes energetically favourable to introduce twist boundaries with a finite

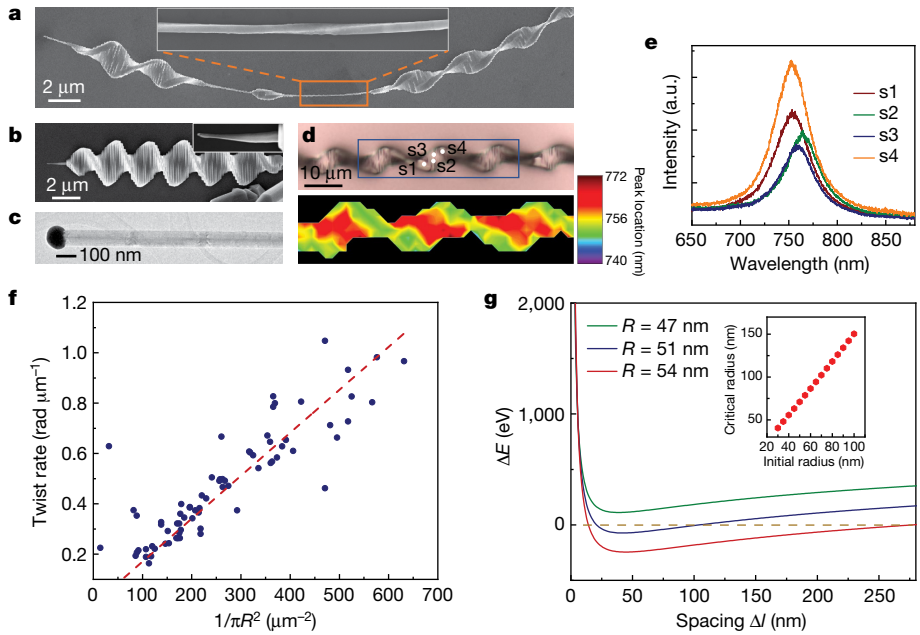

Fig. 4 | Formation mechanism of twisted GeS. a, SEM image of a structure with varying radial size that is formed by non-uniform growth of rotating nanoplates on a twisted nanowire. The inset of **a** highlights the twisting morphology of the nanowire. **b**, SEM image showing a gold nanoparticle at the tip of a mesoscale twisted structure. Inset, the high-magnification SEM image showing the gold nanoparticle (bright spot) at the tip. **c**, TEM image showing the gold catalyst (black particle) at the tip of a dislocated nanowire. **d**, Optical photo of a twisted GeS structure (top) and corresponding photoluminescence spectral maps of peak wavelength position (bottom). The blue frame shows the area for the photoluminescence mapping. **e**, Photoluminescence spectra acquired on spots s1 to s4 marked in **d**, showing the variation of peak position. **f**, Scatterplot of twist rate measured on 73 individual twisted crystals as a function of the inversed contact areas $(\pi R^2)^{-1}$ between gold nanoparticles and the tip. The dashed red line is a least-squares linear fit through the data. **g**, The change in the total energy for a nanowire with twist rate defined at $R_i = 36$ nm, as a function of the spacing between the twist boundaries Δl, for three different values of nanowire radii. The inset shows the change of critical radius as a function of the initial radius of the nanowire, R_i, that defines the twist rate of the pinned structure.

spacing Δl. The critical radius depends on R_i, which defines the twist rate of the pinned nanowire (Fig. 4g); a small initial radius corresponding to a high twist rate results in a small critical radius. The radial size of dislocated nanowires for our growth ranges from 30 nm to 100 nm, giving rise to critical radii from 40 nm to 150 nm.

For further insight into the dependence of the topology on the radial size of the structure, we examined a twisted nanowire pinned on the substrate with a radius of around 150 nm. TEM analysis (Extended Data Fig. 7) confirms that the nanowire possesses twist boundaries at very small twist angles, as well as an almost continuous twisting profile. This very small discrete twisting at the boundaries combined with continuous twisting in the segments between the boundaries is an example of an intermediate twisting state at the onset of formation of the twist boundary. Thus, the 150 nm radial size of the nanowire approximates the critical radius to form the twist boundary. This is in reasonable agreement with the range of critical radii calculated from our theoretical model (Fig. 4g). The result also reveals the gradual transition of the twisting morphology from initial continuous twisting to intermediate twisting (consisting of both continuous twisting between the twist boundaries and discrete twisting at the boundaries) and eventually to discrete twisting with increasing radial size (schematically shown in Fig. 3a, b). This allows us to control the twisting profile and angles at twist interfaces by controlling the radial growth of the structure.

The growth mode identified in GeS is likely to be generic and could be used to produce twisted structure in other vdW materials. To demonstrate its versatility, we synthesized mesoscale germanium selenide (GeSe) structures with discrete twisting by depositing GeSe on the twisted GeS nanowires (Extended Data Fig. 8). In addition, the twisted structures can be transferred to other substrates using a simple wet-transfer method (Extended Data Fig. 9). The bottom-up scheme provides an approach to manipulate the twisting morphology and to realize defect engineering in vdW materials, providing new opportunities to tailor their electrical, optical and thermal properties. Through controlling the radial growth, atomically sharp twist interfaces with a wide and tunable range of twist angles can be created, providing ways to explore 'twistronic' effects in these materials. In addition, the twisting period can be tailored by controlling the diameter of the dislocation-containing nanowires. In contrast to planar and twisted structures, axial structures formed by helical stacking of atomic layers or nanoplates can have a large and modulated chiroptical response due to the periodicity and increased interaction length with light. Moreover, the axial screw dislocation spirally threads the vdW layers, which can improve the electron conductivity along the cross-plane direction[23]. The presence of the dislocation and the twist also enhance the scattering of phonons, lowering the thermal conductivity[28]. The combination of increasing electron conductivity while decreasing thermal conductivity is attractive for thermoelectrics.

Online content

Any methods, additional references, Nature Research reporting summaries, source data, statements of data availability and associated accession codes are available at https://doi.org/10.1038/s41586-019-1308-y.

Received: 8 November 2018; Accepted: 26 April 2019;
Published online 19 June 2019.

1. Kim, C.-J. et al. Chiral atomically thin films. *Nat. Nanotechnol.* **11**, 520–524 (2016).
2. Song, J. C. & Gabor, N. M. Electron quantum metamaterials in van der Waals heterostructures. *Nat. Nanotechnol.* **13**, 986–993 (2018).
3. Cao, Y. et al. Correlated insulator behaviour at half-filling in magic-angle graphene superlattices. *Nature* **556**, 80–84 (2018).
4. Cao, Y. et al. Unconventional superconductivity in magic-angle graphene superlattices. *Nature* **556**, 43–50 (2018).
5. Liu, K. et al. Evolution of interlayer coupling in twisted molybdenum disulfide bilayers. *Nat. Commun.* **5**, 4966 (2014).
6. Naik, M. H. & Jain, M. Ultraflatbands and shear solitons in moiré patterns of twisted bilayer transition metal dichalcogenides. *Phys. Rev. Lett.* **121**, 266401 (2018).

7. Kang, P. et al. Moiré impurities in twisted bilayer black phosphorus: effects on the carrier mobility. *Phys. Rev. B* **96**, 195406 (2017).
8. Shtukenberg, A. G., Punin, Y. O., Gujral, A. & Kahr, B. Growth actuated bending and twisting of single crystals. *Angew. Chem. Int. Ed.* **53**, 672–699 (2014).
9. Jin, S., Bierman, M. J. & Morin, S. A. A new twist on nanowire formation: screw-dislocation-driven growth of nanowires and nanotubes. *J. Phys. Chem. Lett.* **1**, 1472–1480 (2010).
10. Bierman, M. J., Lau, Y. A., Kvit, A. V., Schmitt, A. L. & Jin, S. Dislocation-driven nanowire growth and Eshelby twist. *Science* **320**, 1060–1063 (2008).
11. Zhu, J. et al. Formation of chiral branched nanowires by the Eshelby twist. *Nat. Nanotechnol.* **3**, 477–481 (2008).
12. Oaki, Y. & Imai, H. Amplification of chirality from molecules into morphology of crystals through molecular recognition. *J. Am. Chem. Soc.* **126**, 9271–9275 (2004).
13. Feng, W. et al. Assembly of mesoscale helices with near-unity enantiomeric excess and light–matter interactions for chiral semiconductors. *Sci. Adv.* **3**, e1601159 (2017).
14. Srivastava, S. et al. Light-controlled self-assembly of semiconductor nanoparticles into twisted ribbons. *Science* **327**, 1355–1359 (2010).
15. Eshelby, J. The twist in a crystal whisker containing a dislocation. *Philos. Mag.* **3**, 440–447 (1958).
16. Eshelby, J. Screw dislocations in thin rods. *J. Appl. Phys.* **24**, 176–179 (1953).
17. Sutter, E. & Sutter, P. 1D wires of 2D layered materials: germanium sulfide nanowires as efficient light emitters. *ACS Appl. Nano Mater.* **1**, 1042–1049 (2018).
18. Li, C., Yu, Y., Chi, M. & Cao, L. Epitaxial nanosheet–nanowire heterostructures. *Nano Lett.* **13**, 948–953 (2013).
19. Kong, D. et al. Topological insulator nanowires and nanoribbons. *Nano Lett.* **10**, 329–333 (2010).
20. Peng, H., Xie, C., Schoen, D. T. & Cui, Y. Large anisotropy of electrical properties in layer-structured In_2Se_3 nanowires. *Nano Lett.* **8**, 1511–1516 (2008).
21. Zhang, L. et al. Three-dimensional spirals of atomic layered MoS_2. *Nano Lett.* **14**, 6418–6423 (2014).
22. Shearer, M. J. et al. Complex and noncentrosymmetric stacking of layered metal dichalcogenide materials created by screw dislocations. *J. Am. Chem. Soc.* **139**, 3496–3504 (2017).
23. Ly, T. H. et al. Vertically conductive MoS_2 spiral pyramid. *Adv. Mater.* **28**, 7723–7728 (2016).
24. Tamura, N. in *Strain and Dislocation Gradients from Diffraction: Spatially Resolved Local Structure and Defects* (eds Barabash, R. & Ice, G) 125–155 (Imperial College Press, 2014).
25. Tan, D. et al. Anisotropic optical and electronic properties of two-dimensional layered germanium sulfide. *Nano Res.* **10**, 546–555 (2017).
26. Akatyeva, E., Kou, L., Nikiforov, I., Frauenheim, T. & Dumitrica, T. Electrically active screw dislocations in helical ZnO and Si nanowires and nanotubes. *ACS Nano* **6**, 10042–10049 (2012).
27. Albrecht, M., Lymperakis, L. & Neugebauer, J. Origin of the unusually strong luminescence of a-type screw dislocations in GaN. *Phys. Rev. B* **90**, 241201 (2014).
28. Al-Ghalith, J., Ni, Y. & Dumitrică, T. Nanowires with dislocations for ultralow lattice thermal conductivity. *Phys. Chem. Chem. Phys.* **18**, 9888–9892 (2016).

Acknowledgements Y.L. and J.Y. are supported by the Samsung Advanced Institute of Technology under the grant 037361-003. Work at the Molecular Foundry and the Advanced Light Source was supported by the Office of Science, Office of Basic Energy Sciences, of the US Department of Energy under contract no. DE-AC02-05CH11231. H.S. and D.C.C. are supported by the US Department of Energy, Office of Science, Office of Basic Energy Sciences, Materials Sciences and Engineering Division under contract no. DE-AC02-244 05CH11231 within the Electronic Materials Program (KC1201). This work was performed, in part, at the Center for Nanoscale Materials, a US Department of Energy Office of Science User Facility, and supported by the US Department of Energy, Office of Science, under contract no. DE-AC02-06CH11357. We thank C. So, C. Song, X. Wang, S. Yan, K. Bustillo and C. V. Stan for help with the experiments.

Reviewer information *Nature* thanks Hua Zhang and the other anonymous reviewer(s) for their contribution to the peer review of this work.

Author contributions Y.L. and J.Y. conceived the project and designed the experiments. S.K., Z.F., Y.L. and M.W. synthesized the samples. N.T. performed the X-ray analysis. J. Wang, F.Y., Y.L. and D.J. prepared samples for TEM study. Y.L., J. Wang, J. Wen, K.B.T., X.S. and M.C.S. worked on the TEM measurements. R.Z., Q.Y., J.T., R.O.R. and A.M.M. performed the EBSD analysis. H.S., B.Z.X. and D.C.C. carried out the theoretical calculations. Y.L. and J.Y. wrote the manuscript. All authors discussed the results and commented on the manuscript.

Competing interests The authors declare no competing interests.

Additional information
Extended data is available for this paper at https://doi.org/10.1038/s41586-019-1308-y.
Supplementary information is available for this paper at https://doi.org/10.1038/s41586-019-1308-y.
Reprints and permissions information is available at http://www.nature.com/reprints.
Correspondence and requests for materials should be addressed to J.Y.
Publisher's note: Springer Nature remains neutral with regard to jurisdictional claims in published maps and institutional affiliations.

METHODS

Synthesis. Twisted GeS was synthesized using a horizontal tube furnace with a diameter of 1 inch. The temperature profile of the furnace was measured with a thermocouple. Extended Data Fig. 1 shows a schematic diagram of the furnace and the temperature profiles of the furnace for different heating temperatures at the source site. The substrates used for the synthesis were Si(100) substrates with natural oxidization and thermally oxidized Si(100) substrates with 300 nm silicon oxide. Gold catalyst, 3 nm thick, was deposited on those substrates and was patterned to form microbars in a width of tens of micrometres that are spaced by a few hundred micrometres, using photolithography and electron-beam evaporation deposition. Before the synthesis, the furnace was pumped down to a base pressure of 5 mTorr and flushed with argon gas blended with 4% hydrogen several times. In the synthesis, GeS powder (Sigma-Aldrich) was placed at the centre of the tube and heated to evaporate at a fixed pressure flowing with Ar/4% H_2 carrier gas. The substrates were placed 10–12 cm downstream from the GeS source. Typical growth conditions utilize pressures of 1–2 Torr, flow rates of 20–50 standard cubic centimetres per minute (sccm), source temperatures of 400–450 °C, deposition temperatures of 350–400 °C and a growth time of 20 min.

Characterization. *Laue X-ray microdiffraction analysis.* The crystallinity and orientation of the twisted structures were examined by scanning Laue X-ray microdiffraction (μSXRD) with submicrometre spatial resolution on beamline 12.3.2 of the Advanced Light Source synchrotron at the Lawrence Berkeley National Laboratory. The sample was raster scanned with a 0.5 μm step size and a Laue pattern collected at each step. The Laue patterns were then indexed using the XMAS software, providing orientation map of the sample.

TEM sample preparation. Cross-sectional TEM specimens were prepared from mesoscale and nanoscale twisted GeS structures growing on silicon substrate using a FEI Strata 235 dual beam focused ion beam (FIB) system and an FEI Nova 600 FIB. Low-energy argon ion milling at 900 eV was further used to minimize sidewall damage and to thin the specimen for electron transparency. Free-standing nanowires that grew vertically on the substrate were mechanically transferred to copper TEM grids for TEM analysis.

Electron microscopy. SEM imaging was performed using a Zeiss Gemini Ultra-55 Analytical SEM. Electron backscattering diffraction (EBSD) was performed in a FEI Strata 235 dual beam FIB at 20 keV using an equipped EBSD detector. EBSD orientation maps were generated and analysed using OIM software. TEM analysis was performed using a FEI TitanX, a JEOL 3010 in situ TEM, an Argonne Chromatic Aberration-corrected TEM (ACAT), and a FEI Titan 80-300 ST with both spherical and chromatic aberrations correctors. Atomic resolution HAADF-STEM images were acquired using the monochromated, aberration-corrected TEAM 0.5 TEM at the Lawrence Berkeley National Laboratory, operating at 200 keV.

Optical characterization. Photoluminescence measurements and mapping were conducted using a Horiba Jobin Yvon LabRAM ARAMIS automated scanning confocal Raman microscope under 532 nm excitation.

Theoretical model. The periodicity of the twist boundaries in the nanowires can be explained using a simple model rooted in the Eshelby twist[16] and the associated strain energy, the fact that the nanowires are adhered to the substrate, and the notion of a critical thickness for misfit dislocations to arise.

We can build a semiquantitative model for the process to estimate the spacing of the twist boundaries. We assume that the nanowire can, at all times, be modelled as a cylindrical wire with radius R. The wire grows very rapidly in the initial stages, owing to the VLS process and the screw dislocation along the wire axis. The radius of the nanowire at this stage is assumed to be R_i. Growth to radii beyond that of the gold droplet, however, is much slower, and is mediated by direct deposition. The screw dislocation along the axis of the nanowire introduces a net torsion into the wire, and this torsion leads to the so-called Eshelby twist[16], where the twist rate of the wire, α, is given by:

$$\alpha = \frac{b_a}{\pi R_i^2} \tag{1}$$

where b_a is the Burgers vector of the axial screw dislocation.

In the initial growth process, the wire comes into contact with the substrate and bonds to it. The result of this bonding is that the total twist rate of the wire is fixed at α throughout the remainder of the growth process. As the radius of the wire increases during the growth, the equilibrium twist rate is reduced below that of equation (1). However, since the wire has a net twist rate given by equation (1), this leads to an excess of torsional strain energy stored in the wire. We hypothesize that this excess strain energy can be reduced by the introduction of twist boundaries into the nanowire. These twist boundaries can reduce the torsional strain energy in the cylinder but introduce an array of misfit dislocations to define the twist boundary. The interplay between these two effects can define the critical thickness separating twist boundaries[29]. The critical distance so defined represents a lower limit on the spacing of the twist boundaries, as kinetic effects might lead to larger spacings than those predicted by the model.

We will first assume that we can model the nanowire as a cylinder of radius R that is growing along the z-direction. The total change in elastic energy upon introducing twist boundaries with a spacing Δl can be computed. The twist boundaries are defined by two perpendicular arrays of screw dislocations that are introduced into the wire in crossed pairs. The introduction of n pairs of dislocations, each with Burgers vector of length b_m, at a spacing $d = \frac{2R}{n}$ within the plane of the twist boundary creates a twist boundary with the twist angle, θ, given by[30]:

$$\theta = \frac{b_m}{d} = \frac{b_m}{2R} n \tag{2}$$

We then note that the change in elastic energy $\Delta E_{elastic}$, in a wire of length Δl, upon introducing the twist boundary described by equation (2) is given by:

$$\Delta E_{elastic} = -n\frac{b_a\, b_m K_s R^3}{4R_i^2} + n^2 \frac{b_m^2 K_s\, \pi R^2}{16\, \Delta l} \tag{3}$$

Here K_s is the torsional shear modulus of the material.

The reduction in elastic energy, equation (3), is countered by the introduction of n pairs of misfit dislocations. The energy of these dislocations E_{dis} is taken to be, approximately,

$$E_{dis} = n\frac{R}{\pi} K_e b_m^2 \log\left(\frac{\Delta l}{\beta b_m}\right) \tag{4}$$

with βb_m the core radius of the misfit dislocations defining the twist boundary, and K_e the elastic constant governing the line energy of the dislocation computed from anisotropic elasticity theory[30–32]. For simplicity, we take both sets of screw dislocations defining the twist boundary to have the same Burgers vector, and we assume that all have the same length, $2R$. (GeS is orthorhombic, so the screw dislocations in question have slightly different lengths of Burgers vectors. We choose the shorter of the two vectors, and the spacing is then that associated with the smallest of the Burgers vectors. For a pure twist boundary, the ratio b_m/d is fixed to be the same constant for both sets of dislocations.)

These two contributions can be summed to give the total change in energy upon introduction of a twist boundary with n pairs of misfit dislocations[29] at intervals of Δl. We choose to measure all lengths in terms of b_m, all elastic constants in terms of K_s and all energies in units of $K_s b_m^3$. In non-dimensional form, the expression for the change of energy, ΔE_{tot}, for a wire of radius R with twist rate fixed at a radius R_i, becomes:

$$\Delta E_{tot} = \frac{1}{16} nR\left(R\left(-\frac{4b_a R}{R_i^2} + \frac{n\pi}{\Delta l}\right) + \frac{16}{\pi} K_e \log\left[\frac{\Delta l}{\beta}\right]\right) \tag{5}$$

where all variables now refer to their dimensionless versions.

Equation (5) enables exploration of the relationship between twist boundary spacing and the materials properties. There are only three constants that appear in equation (5): β, b_a and K_e. The parameter β defines the core radius of the misfit dislocations. Typically, one expects β to be the order of 1, and we choose to set $\beta = 1$. The in-plane lattice parameters of GeS (according to the Materials Project Database[33]) are given by $a = 0.36$ nm and $b = 0.44$ nm. We choose a to set our length scale. With this choice, the dimensionless axial Burgers vector length becomes $b_a = 2.889$.

We begin by considering ΔE_{tot} as a function of Δl, at fixed values of R_i and R. Determination of the exact value for K_e is beyond the scope of this project. On the basis of rough calculations, we estimate that $K_e = 3/4$. Extended Data Fig. 10 displays the change in total energy for a cylinder with dimensionless twist radius defined at radius $R_i = 100$ (that is, 36 nm, comparable to the experiment) for three different values of R. Note that there is a critical value for R at which it becomes possible to introduce the misfit dislocations. When R exceeds this value, the dislocations can be introduced over a finite range of Δl. This unusual dependence is simple to understand. For small Δl, the twist rate is markedly decreased through the introduction of a single twist boundary. However, as Δl grows, the average twist rate reduction due to each twist boundary decreases. The result is that if Δl is too large, the reduction in torsional strain energy due to a single twist boundary cannot be large enough to generate the dislocations of the twist boundary.

The critical Δl values predicted by the model at the critical R are too small, hovering near 30 nm, whereas the experiment indicates values nearer to 200 nm. There are many potential origins for this discrepancy, but we believe that the kinetics of misfit dislocation introduction are the most important. Consider a cylinder, again with the twist radius initially fixed at $R_i = 100$ (in unit of b_m). As it grows below the critical radius, there is no driving force to create any twist boundary, since introducing a twist boundary always increases the energy. However, as the cylinder slightly exceeds the critical radius (for example $R = 140$), a twist bound-

ary can be introduced, and for a larger radius ($R = 150$), it is possible to have separations up to approximately 800 (in dimensionless units) between twist boundaries while still reducing the total energy. On reinserting dimensions into these equations, the model predicts that twist boundaries can be introduced into the nanowire when its radius approaches 50 nm. By the time the wire is 54 nm in radius, the critical spacing range over which a twist boundary would be stable, Δl, includes thicknesses ranging from 18 nm to 288 nm. It is likely that introduction of the misfit dislocations to create the twist boundaries will require the overcoming of kinetic limitations, and that the nanowire will continue to grow radially while these kinetic limitations are being overcome. Given the sensitivity to the radius of the wire and the simplicity of the model, the separations agree well with the experimental observations.

Data availability

All data supporting the findings of this study are available within the paper.

29. Ertekin E., Greaney, P. A., Chrzan, D. C. & Sands, T. D. Equilibrium limits of coherency in strained nanowire heterostructures. *J. Appl. Phys.* **97**, 114325 (2005).
30. Hirth, J. P. & Lothe, Jen. *Theory of Dislocations* (Krieger, 1992).
31. Eshelby, J. D., Read, W. T. & Schockley, W. Anisotropic elasticity with applications to dislocation theory. *Acta Metall.* **1**, 251–259 (1953).
32. Foreman, A. J. E. Dislocation energies in anisotropic crystals. *Acta Metall.* **3**, 322–330 (1955).
33. de Jong, M. et al. Charting the complete elastic properties of inorganic crystalline compounds. *Sci. Data* **2**, 150009 (2015).

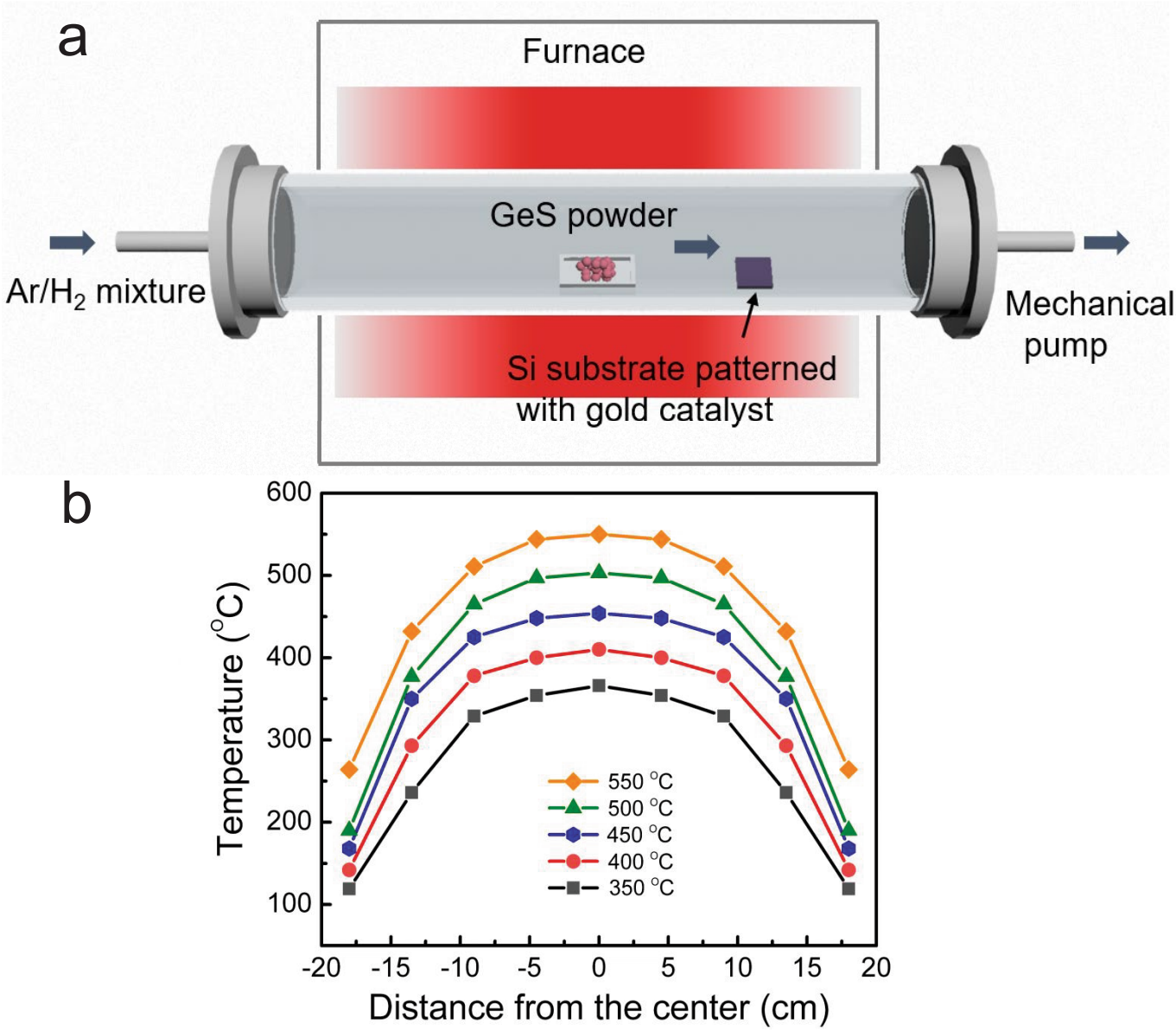

Extended Data Fig. 1 | Furnace set-up for the growth. a, Schematic diagram of the furnace used for the synthesis of the twisted GeS crystals. **b**, Temperature profiles of the furnace for heating temperatures of 350 °C, 400 °C, 450 °C, 500 °C and 550 °C at the source site.

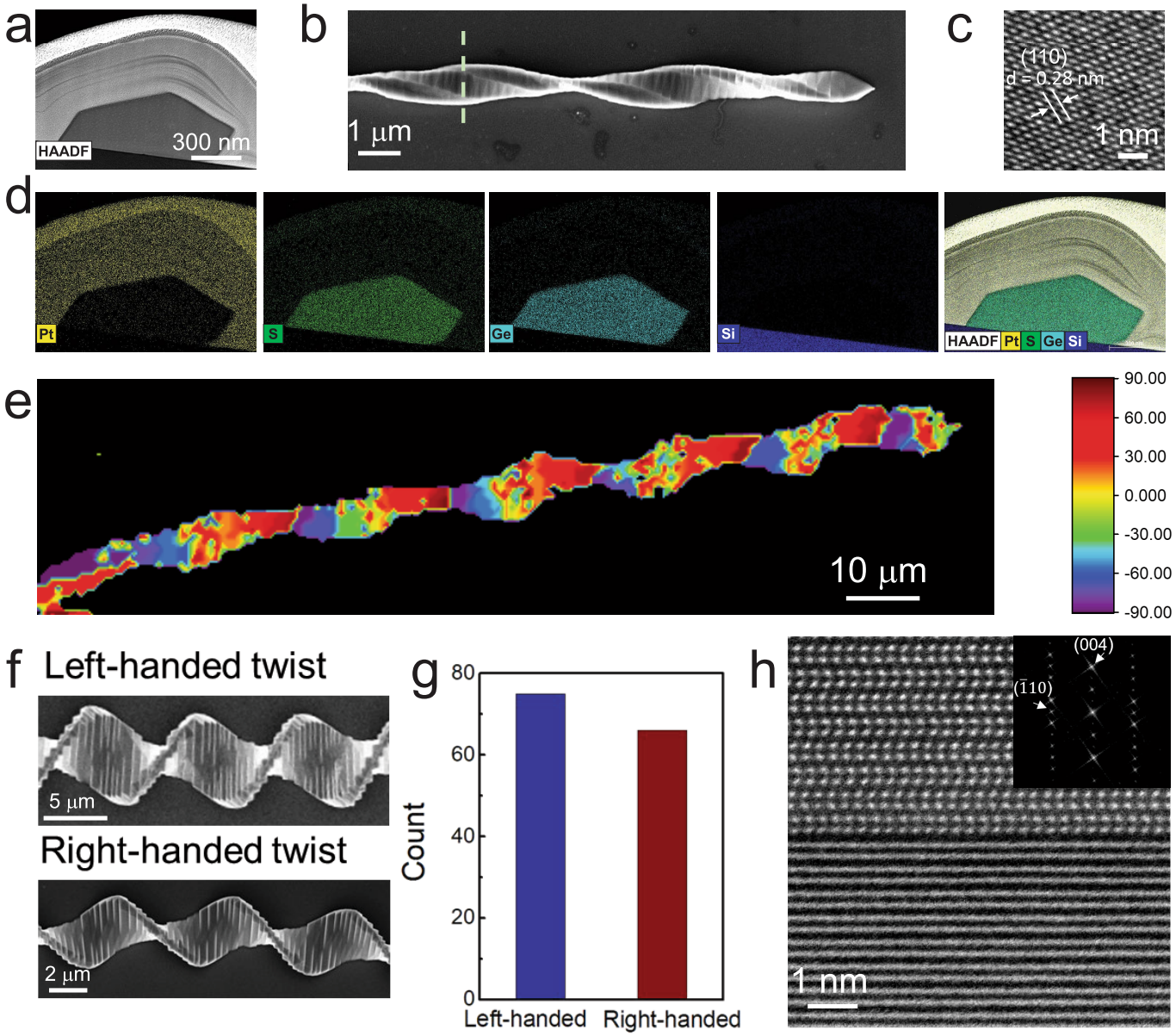

Extended Data Fig. 2 | Additional chemical and structural analysis of mesoscale twisted GeS. a–d, Chemical analysis of mesoscale twisted GeS using energy-dispersive X-ray spectroscopy (EDS). **a**, HAADF-STEM image of a cross-sectional lamellar sample with its normal perpendicular to the twist axis prepared by FIB milling. **b**, SEM image showing the crystal used to prepare the TEM sample. The dashed line represents the location of the cross-section. **c**, High-resolution TEM (HRTEM) image of the cross-section confirming that the twist axis is aligned with the [001] direction. **d**, STEM-EDS elemental map of the cross-section verifying that the structure is a compound consisting of Ge and S in an atomic ratio of 1:1. **e**, Additional X-ray microdiffraction analysis on a twisted GeS crystal with a period of about 15 μm. The orientation angle in the X-ray orientation map is defined by the angle between the *b* axis and the normal to the substrate. The large period, corresponding to a low crystallographic twist, facilitates the use of X-ray microdiffraction to determine the crystal orientation. The X-ray analysis also suggests that the widest portion in a period has its *b* axis aligned with the substrate normal while the narrowest portion in the period has its *a* axis aligned with the substrate normal. This growth phenomenon may result from the structural anisotropy of GeS. **f**, **g**, Handedness of mesoscale twisted GeS. **f**, Representative SEM micrographs showing twisted structures with opposite helicity. **g**, Histogram showing that the population of left-handed structures is approximately equal to the population of right-handed structures. The measured ratio of left-handedness to right-handedness is 74:67. **h**, Additional atomic-resolution HAADF-STEM image of a twist interface in a twisted GeS structure with the upper crystal oriented on the [110] zone axis. The inset shows the FFT pattern of the upper crystal.

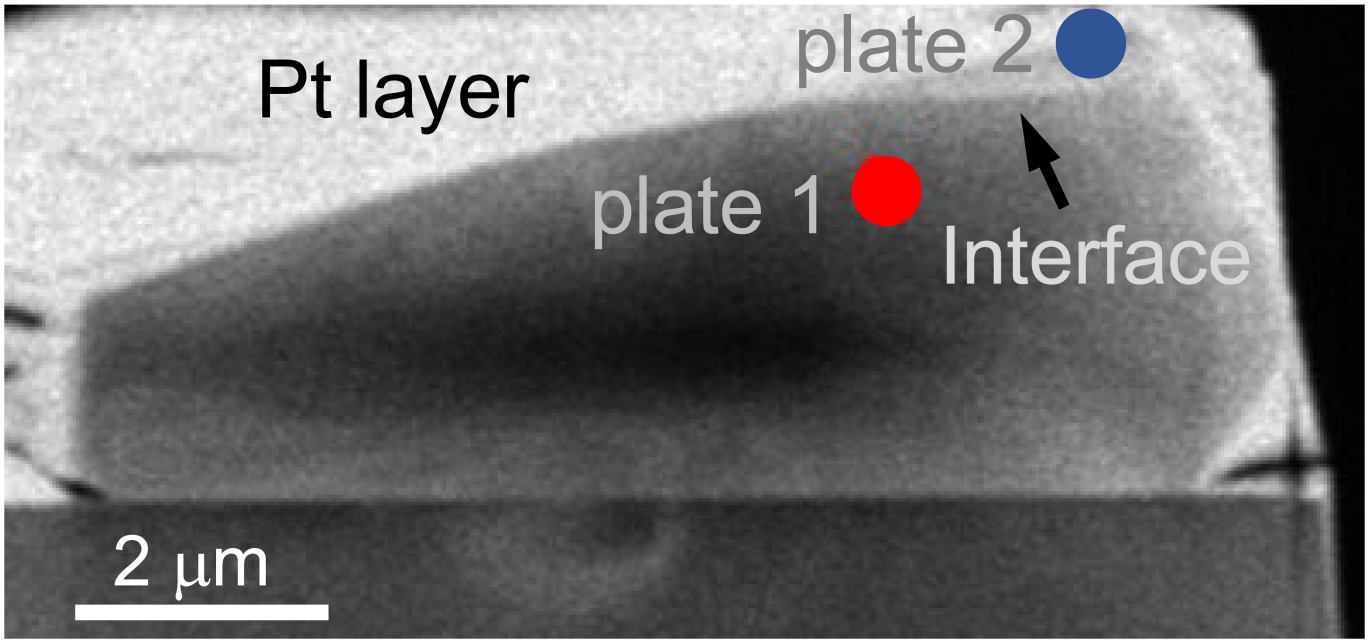

Extended Data Fig. 3 | TEM image of the specimen on which diffraction patterns in Fig. 2c–e were obtained. Using FIB, a lamellae sample containing two adjacent stacking nanoplates was prepared with the surface normal along the twist axis. After the thinning of the sample, the largest fraction of the sample consists of a single nanoplate (either the top or the bottom one), while a smaller fraction preserves the twist interface between the two nanoplates. The arrow shows the location of the twist interface. The red and blue dots show the locations that respectively contain the single upper plate and the single lower plate.

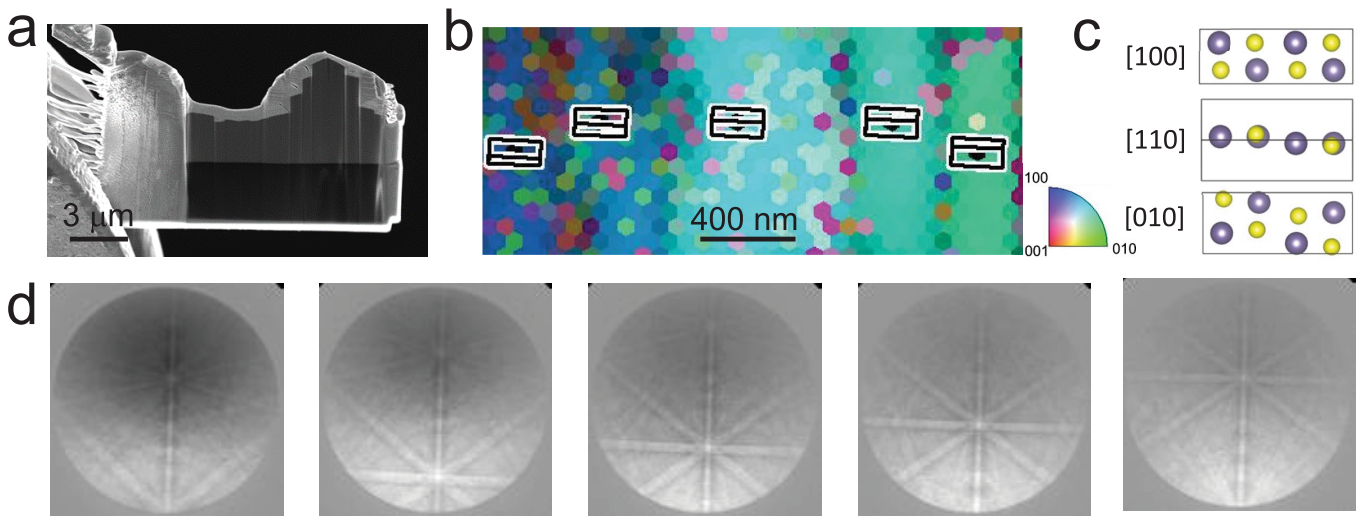

Extended Data Fig. 4 | Electron backscattering diffraction analysis. **a**, SEM image of a specimen used for EBSD. The lamellar sample is prepared by FIB milling with surface normal perpendicular to the twist axis of the structure. **b**, Representative EBSD orientation map of the nanoplates with the 2D projection of the unit cell superimposed. The unit cell projection shows the crystal orientation of the nanoplates at that point. The misorientations of the plates (that is, the differences between the crystal orientations of adjacent nanoplates) are quantified to be 10.2°, 14°, 6.7° and 8.7°. **c**, Unit cell of GeS viewed along the [100], [110] and [010] directions. **d**, Corresponding EBSD patterns acquired from five adjacent nanoplates. Note that 13 twist angles were measured on four mesoscale twisted structures using EBSD, and a representative measurement is shown in this figure. In addition, two twist angles were measured using the TEM (shown in Fig. 2). In total, 15 twist angles were measured on six twist structures. The values of the measured twist angles are 10.6°, 16°, 6.8°, 10.3°, 13.9°, 7.1°, 8.3°, 14°, 9.6°, 10.2°, 14°, 6.7°, 8.7°, 10.27° and 7.5°. This is a range from 6.8° to 16° with an average of 10.3° and standard deviation of 3°.

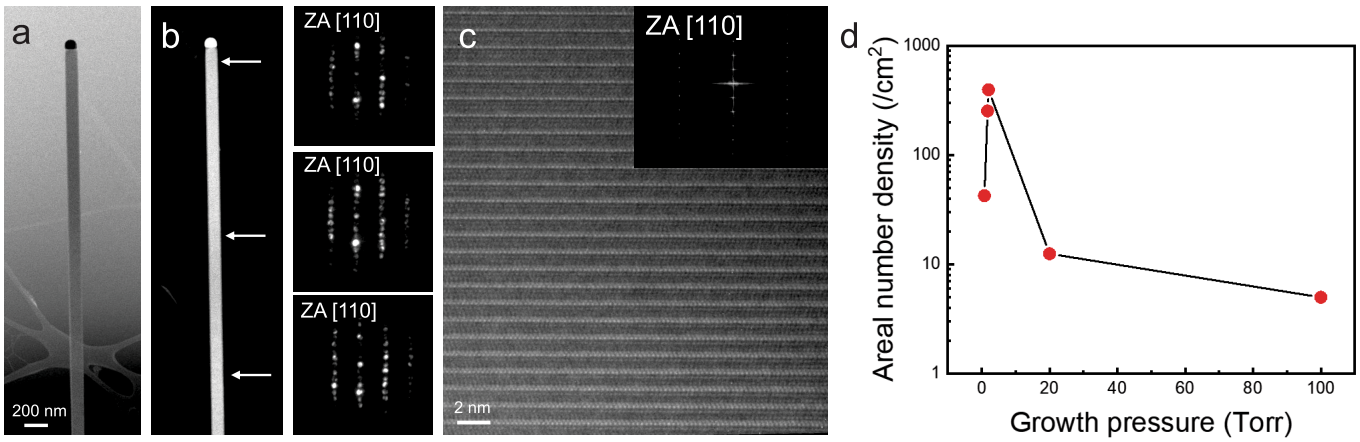

Extended Data Fig. 5 | The effect of growth pressure on the growth of dislocated nanowires. a, TEM image of a normal nanowire without a dislocation produced at a growth pressure of 5 Torr. **b**, Corresponding STEM image of the nanowire (left) and CBED patterns acquired from three different locations on the nanowire (right), showing the absence of the Eshelby twist. The white arrows in the STEM images show the locations where the CBED patterns are collected. **c**, HRTEM image of the normal nanowire showing that the growth direction of the nanowire is along the *c* axis. The inset is the FFT pattern of the HRTEM image suggesting the image is taken on the [110] zone axis (ZA). **d**, Areal number density (the number of twisted structures per unit area of the substrate) of twisted GeS structures as a function of the growth pressure. In this experiment, the flow rate of Ar/H_2 carrier gas and the source temperature were fixed at 50 sccm and 450 °C, respectively. The growth of dislocated nanowires is achieved with typical growth pressures in the range 1–2 Torr and a flow rate of 20–50 sccm, whereas the yield of nanoscale and mesoscale twisted GeS drops when the growth pressure deviates from optimum.

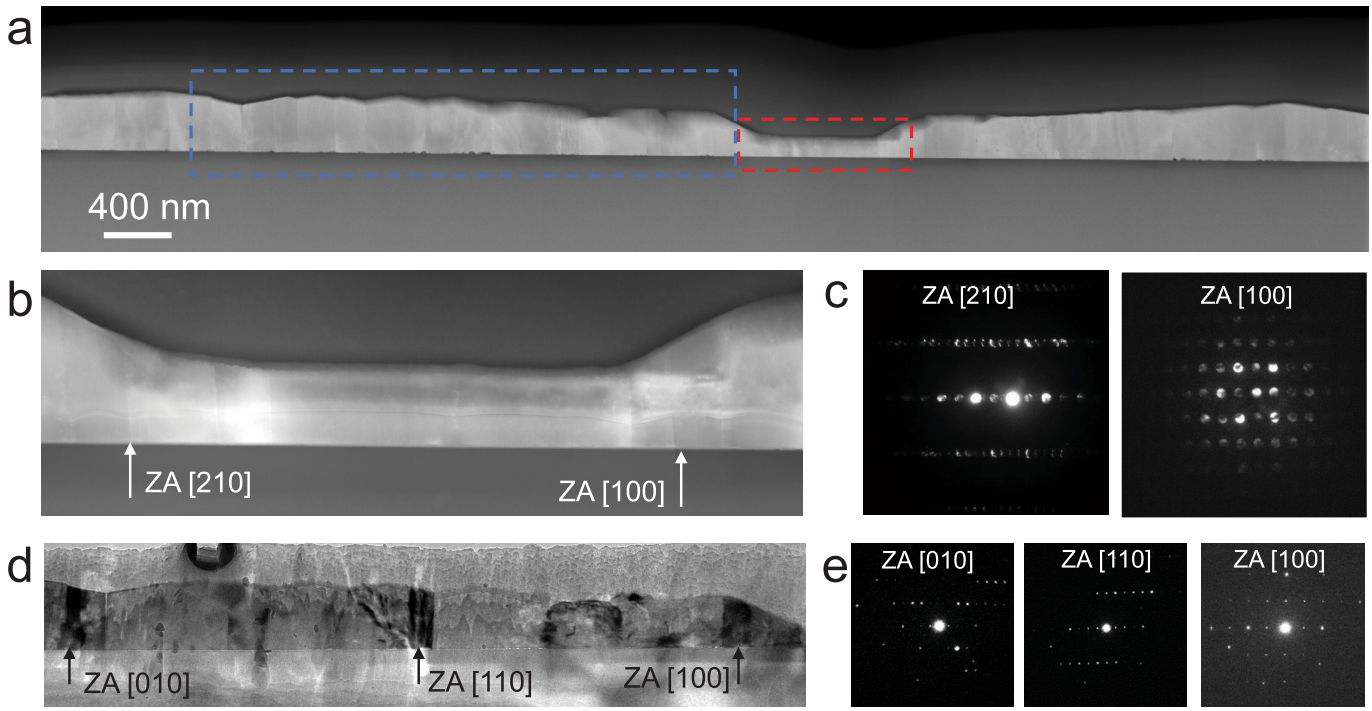

Extended Data Fig. 6 | The invariance of the total twist rate in the radial growth of a pinned structure. a, STEM image of a cross-sectional sample prepared from a twisted structure pinned on a substrate. This twist structure was formed by non-uniform radial growth on a twisted nanowire (similar to the structure shown in Fig. 4a), showing varying radial sizes for different portions of the structure. To verify the invariance of the total twist rate in the radial growth of a pinned structure, we used electron diffraction to measure the twist rates of different portions with varying radial sizes in the structure. **b**, Magnified STEM image of a thin portion highlighted by the dashed red box in **a**. **c**, CBED patterns for the [210] and [100] zone axes collected at locations marked by arrows in **b**. This suggests that the thin portion has a twist of 23° over a length of 970 nm, amounting to a twist rate of 0.4 rad mm^{-1}. **d**, Magnified TEM image showing a thick portion highlighted by the dashed blue box in **a**. **e**, SAED patterns for the [010], [110] and [100] zone axes collected at locations marked by arrows in **d**. This suggests that the thick portion has a twist of 90° over a length of 4 μm, giving rise to a twist rate of 0.4 rad mm^{-1} as well. This electron diffraction analysis shows that twist rates at different portions with varying radial sizes in the structure are almost same, despite the significant difference in their radial size. Note that the thick portion has a radial size (about 450 nm) two times larger than that of the thin portion (about 150 nm). This result suggests that the overall twist rate of the structure is determined by the twist rate of the nanowire upon substrate pinning, and further radial growth does not result in untwisting that decreases the twist rate. The high twist rate of the initial nanowire with Eshelby twist is therefore preserved during radial growth.

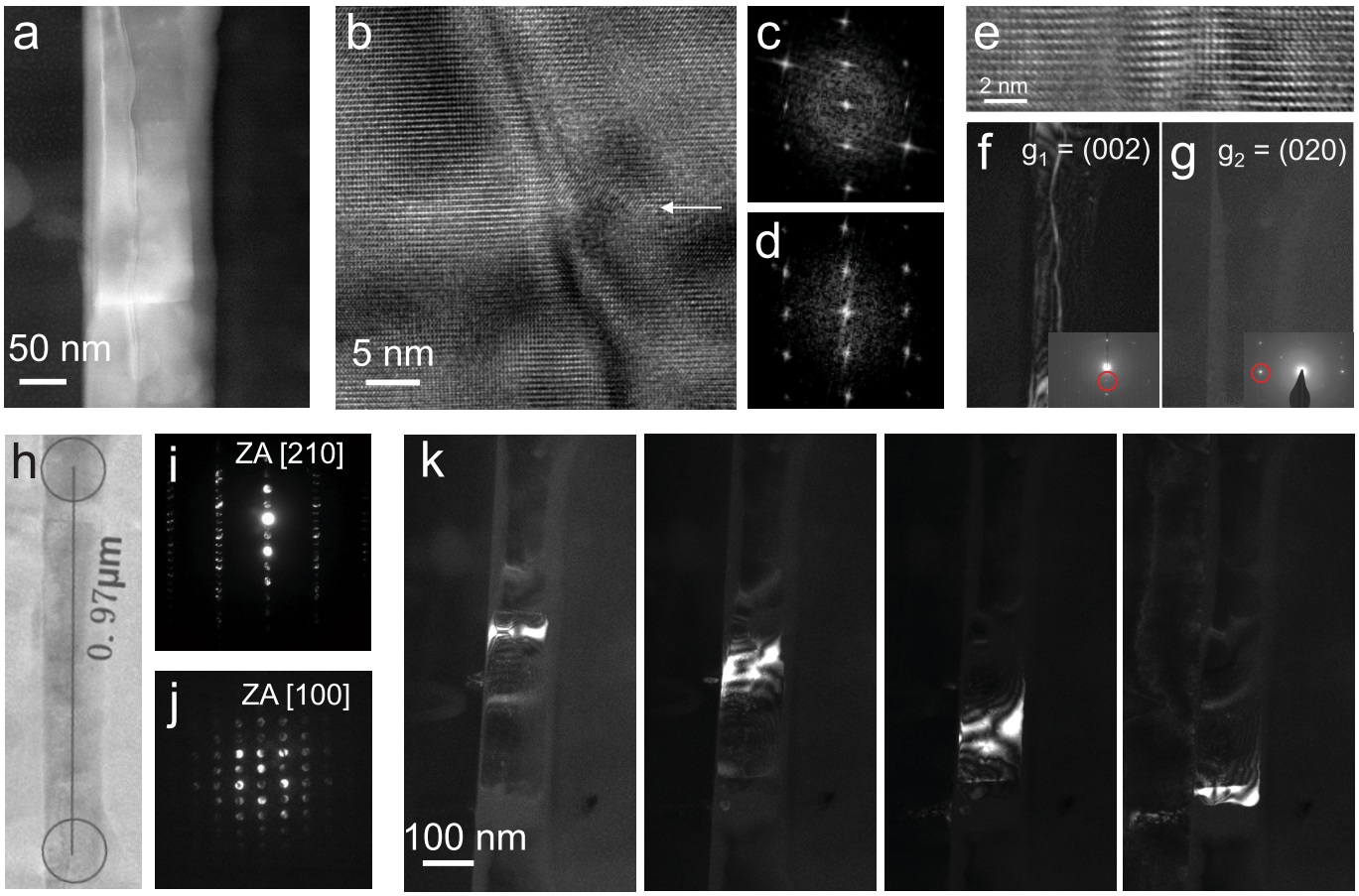

Extended Data Fig. 7 | Twisted GeS nanostructure in an intermediate twisting state. a, Low-magnification STEM image of a nanostructure growing horizontally on a substrate. The nanowire had an approximate radial size of 200 nm and height of 150 nm with a twisting morphology that can be clearly observed by SEM imaging. We note that this nanostructure is the thin part of the sample shown in Extended Data Fig. 6. In contrast to free-standing nanowires (Fig. 3d) that have only a screw dislocation, the nanowire was segmented with the presence of both transverse boundaries and a dislocation line in the middle. **b**, HRTEM view of a boundary. The white arrow shows the boundary. **c**, **d**, FFT pattern of the two crystals across the boundary. The HRTEM imaging and the corresponding FFT patterns confirm that the crystals across the boundary have almost the same orientation and thus the boundary takes on a very small twist angle. **e**, HRTEM image of the screw dislocation. **f**, **g**, Burgers vector analysis, based on the $\boldsymbol{g} \cdot \boldsymbol{b}$ contrast. To perform the analysis, the nanowire was first tilted to the [100] zone axis. Next, the sample was further tilted to create two-beam conditions for different diffraction spots in the diffraction pattern. Dark-field images of the dislocation were taken for $\boldsymbol{g} = (002)$ (**f**) and $\boldsymbol{g} = (020)$ (**g**). The insets show the excitation of reflections for the dark-field imaging in which the selected reflections are marked with red circles. For $\boldsymbol{g} = (002)$, high contrast of the dislocation is observed in the dark-field image (**f**), whereas for $\boldsymbol{g} = (020)$, the dislocation becomes invisible in the image (**g**). We have therefore determined the Burgers vector of the dislocation to be along the [001] direction, which is the same as for the dislocated nanowires that were grown vertical and free-standing. **h**, Low-magnification cross-sectional TEM image of the nanowire. **i**, **j**, CBED patterns for the [210] and [100] zone axes are collected at locations marked by circles in **a**, which were separated by 970 nm. This suggests a twist of 23° about the *c* axis within this length, amounting to a twist rate of 0.4 rad mm^{-1}, which is comparable to the twist rate of mesoscale crystals. **k**, A series of dark-field TEM images showing that the [020] diffraction band progressively shifts when the sample is continuously rotated about its twist axis by tilting the TEM holder; this dark-field imaging verifies that the crystallographic twist of the nanowire is almost continuous. As such, the nanostructure has both twist boundaries with very small twist angles and an almost continuous twisting profile, exemplifying an intermediate twisting state at the onset of formation of the twist boundary.

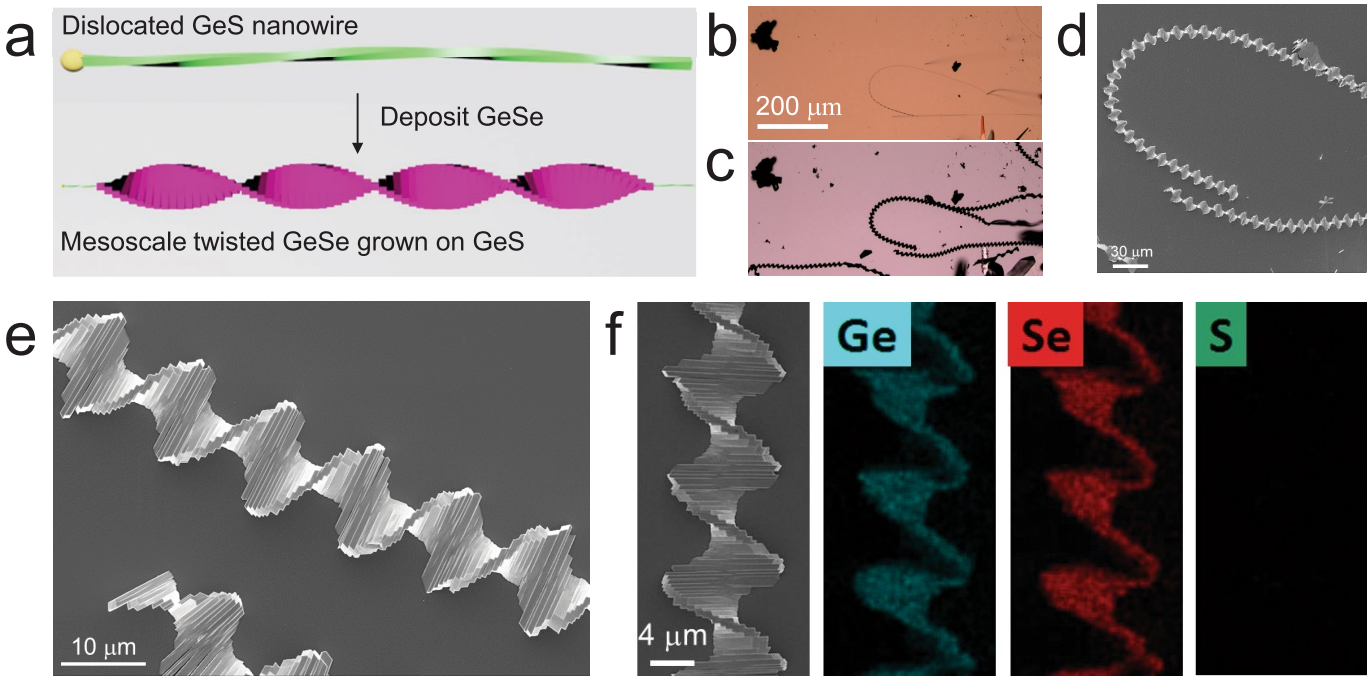

Extended Data Fig. 8 | Synthesis of mesoscale twisted GeSe using dislocated GeS nanowires as seeds. a, Schematic showing the synthesis of mesoscale twisted GeSe structures. Twisted GeS nanowires were first grown via the VLS method. In a second growth, GeSe was deposited on the GeS nanowires using the chemical vapour transport method. **b**, Optical image of dislocated GeS nanowires. **c**, Optical image of mesoscale twisted structures synthesized through depositing GeSe on those twisted GeS nanowires. **d**, **e**, SEM images of twisted GeSe structures at low magnification (**d**) and at high magnification (**e**). **f**, SEM image (left) and corresponding EDS elemental maps of the structure. Quantitative chemical analysis using EDS suggests an almost 1:1 atomic ratio of Ge to Se.

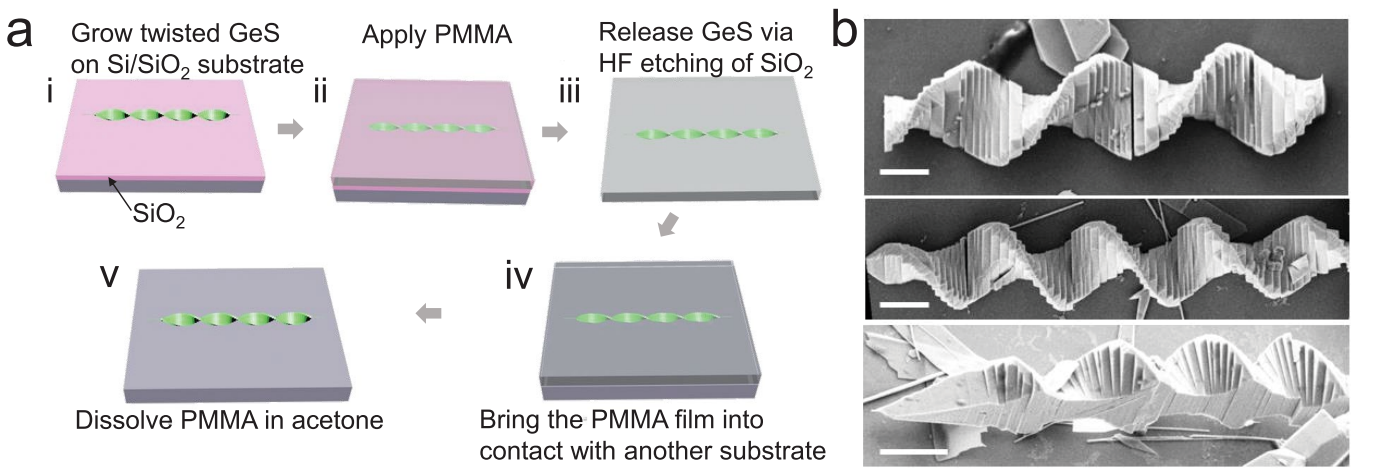

Extended Data Fig. 9 | Transfer of twisted GeS crystals to other substrates. a, Schematic showing a facile processing scheme to transfer twisted GeS crystals to other substrates. i, Twisted crystals were first grown on a thermally oxidized Si/SiO_2 substrate. These crystals adhered well to the substrate. ii, Polymethyl methacrylate (PMMA) was applied on the substrate. iii, The SiO_2 layer was etched using hydrofluoric acid, and the crystals were transferred to the PMMA film. iv, The PMMA film with the crystals was brought into contact with another substrate. v, The GeS crystals were transferred to the substrate by dissolving PMMA in acetone. **b**, SEM images of the GeS crystals after the transfer. Scale bar, 4 μm.

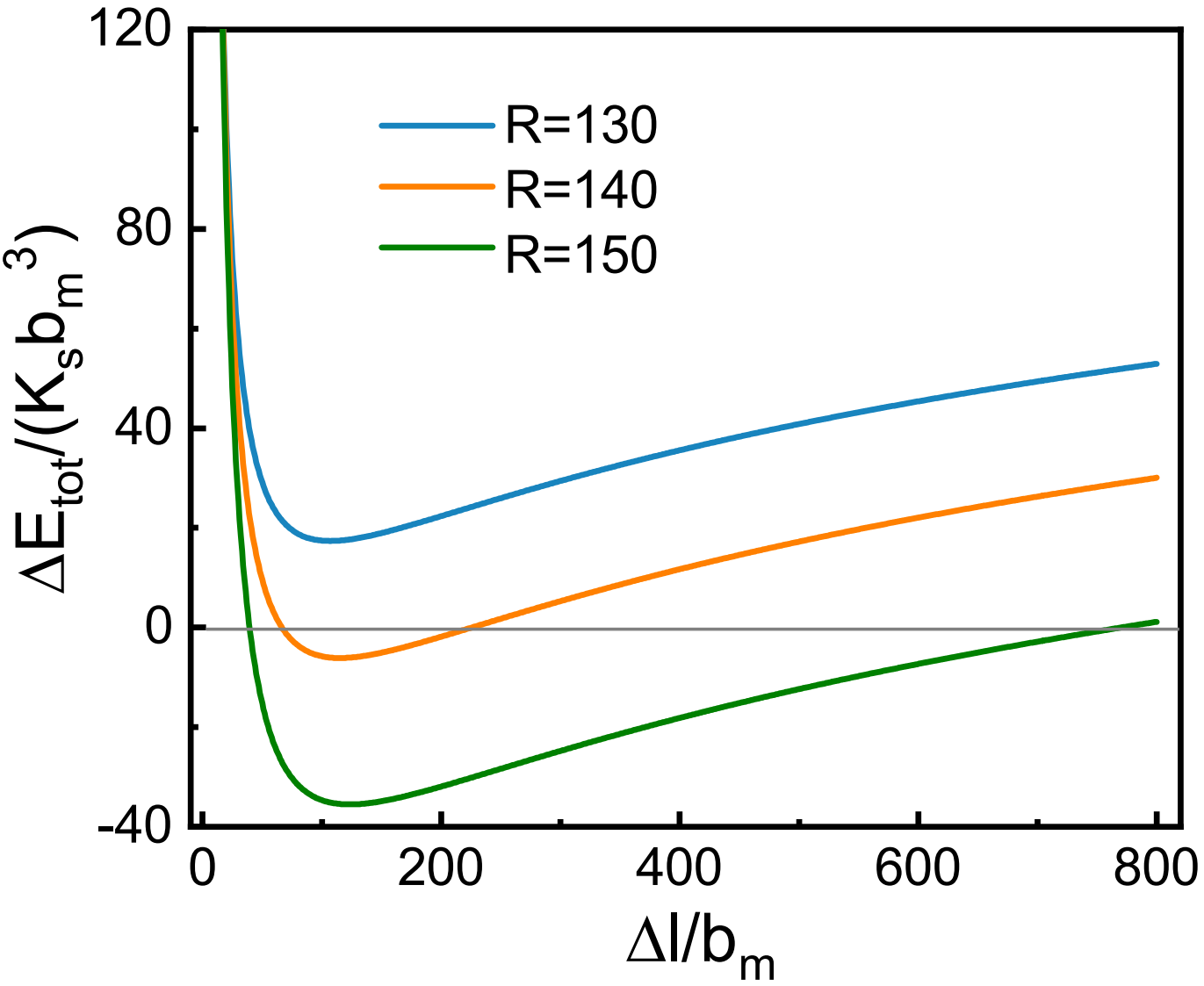

Extended Data Fig. 10 | Change in energy. The total change in energy upon introduction of one dislocation pair into a nanowire of radius R (dimensionless), given that the initial twist rate of the wire is set at $R_i = 100$. Note that for these conditions there is a critical value of R necessary to introduce misfit dislocations, as well as a critical thickness. Note also that the energy is only reduced over a range of Δl. See Methods for details.